Cohesive Zone Model for Surface Cracks using Finite Element Analysis

De Xie, Mohit Garg, Dade Huang, and Frank Abdi

Alpha STAR Corporation
5199 E Pacific Coast Highway, Suite 410
Long Beach, CA 90804, USA

Abstract

A debonding comparative study for accuracy and software convergence among the Finite Element based non-predetermined crack growth strength/strain based Progressive Failure Analysis (PFA) and pre-determined crack growth fracture mechanics based Continuous/Discrete cohesive zone model (CZM) is performed. It is concluded that for typical 2D/3D crack growth or debonding, a combination of PFA and CZM will result in then most accurate predicted load-displacements in comparison with test. PFA requires the fiber/matrix or lamina material input and is mesh sensitive at the crack tip, necessitating a mesh convergence effort. PFA generates an accurate crack path and the load displacement curve (up-to load peak value). Continuous/Discrete CZM requires the fracture toughness, correlation of cohesive strength and predetermined crack path/interfaces. Several comparative studies of these methodologies against test data were performed. In particular the Composite Storage Module (CSM) adhesively bonded joint tests revealed the pre-mature failure of the bonded area as possible combination of both adhesive and cohesive failure. Adhesive joint failure was caused by a) non-clean surface preparation, b) thick bond line, and c) existence of voids in the adhesive bondline. The problem was analyzed using two approaches: a) Progressive failure analysis with complete and partial bond void representation and b) Virtual Crack Closure Technique with complete and partial bonding. Results indicated full load carrying capability of the joint using PFA and VCCT and a complete bondline approach and a significant reduction in the load carrying capability due to improper bonding.

Nomenclature

PFA = Progressive Failure Analysis
CCZM = Continuous cohesive zone model
DCZM = Discrete cohesive zone model
VCCT = Virtual crack closure technique
SERR = Strain energy release rate,
σ_c = cohesive strength
K_{IP}=Cohesive stiffness
G_c = Fracture energy
δ_m = Maximum separation beyond which a stress free surface is formed
K_x, K_y, K_z = Spring stiffness in X, Y, Z global directions

1. Introduction

Debonding of adhesively bonded joints and delamination of composite materials are major concerns in aero structures. To study the problem, fracture mechanics based approach can be used for sharp crack of linear elastic materials. As to the energy-based criterion (strain energy release rate, SERR), the virtual crack closure technique (VCCT) is a powerful tool to compute SERR by using finite element analysis (FEA). Some applications of VCCT to study the crack growth can be found in [1-7].

However, in reality, neither the idealized sharp crack nor the linear elastic material does exist. This is particular true for composite materials and adhesively bonded joints. Therefore, recently, using of cohesive zone model (CZM) is increasing. The idea of CZM is straightforward. It is a natural extension of BD model, which was proposed for perfect plastic materials. However, the implementation of CZM with FEA varies. There are two major classes: continuum cohesive zone model (CCZM) and discrete cohesive zone model (DCZM) [8-11]. Let's use pure mode I case to address the major differences between CCZM and DCZM.

In CCZM, an energy potential function $\phi(\delta)$ is needed to construct the constitutive equation. Then, the interface tractions are:

$$\sigma = \frac{\partial \phi}{\partial \delta} \qquad [1]$$

For mode I, one of the earliest energy potential functions was assumed to be a polynomial proposed by Needleman [12,13] as:

$$\phi(\delta) = \frac{27}{4}\sigma_c \left\{ \frac{1}{2}\left(\frac{\delta}{\delta_m}\right)^2 \left[1 - \frac{4}{3}\left(\frac{\delta}{\delta_m}\right) + \frac{1}{2}\left(\frac{\delta}{\delta_m}\right)^2 \right] \right\} \qquad [2]$$

Thus the normal traction for this potential is

$$\sigma = -\frac{27}{4}\sigma_c \left\{ \left(\frac{\delta}{\delta_m}\right) \left[1 - 2\left(\frac{\delta}{\delta_m}\right) + \left(\frac{\delta}{\delta_m}\right)^2 \right] \right\} \qquad [3]$$

where σ_c is the cohesive strength and δ_m is the maximum separation beyond which a stress free surface is formed. Both σ_c and δ_m can only be determined from experimental calibration. Many other forms of energy potential function $\phi(\delta)$ have been proposed [13, 14]. From numerical point of view, if $\phi(\delta)$ is not assumed well, the CCZM may have convergence difficulties [15].

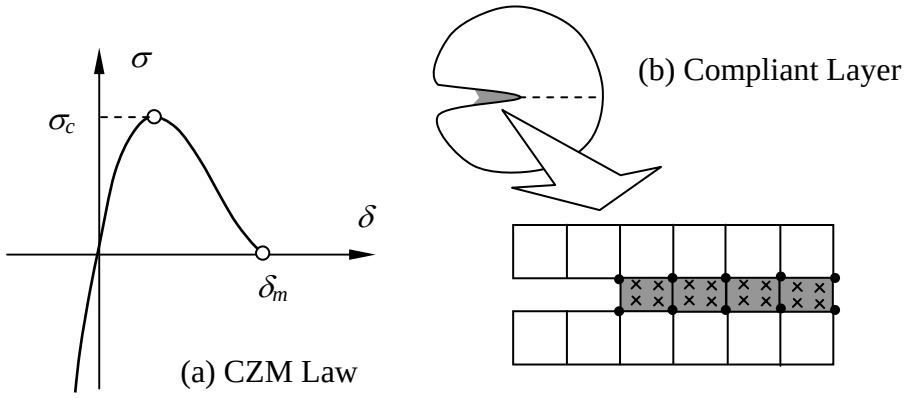

Figure 1. Continuum Cohesive Zone Model (CCZM)

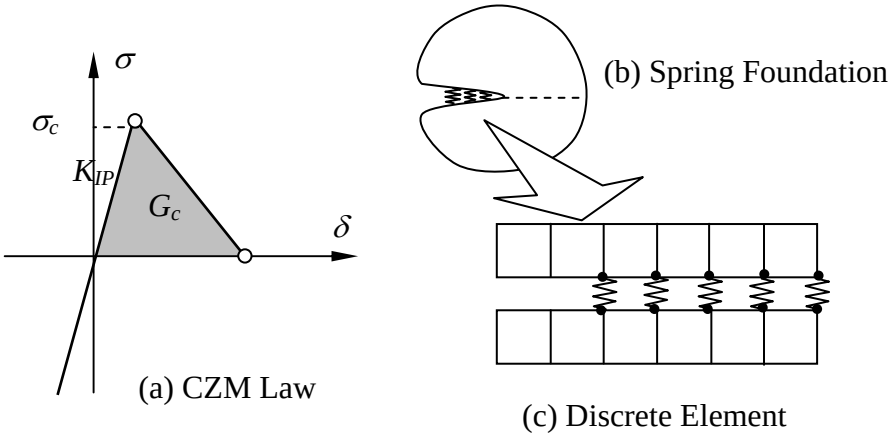

Figure 2. Discrete Cohesive Zone Model (DCZM)

In DCZM, the energy potential function $\phi(\delta)$ is not needed. The CZM law is directly constructed based on the experimental calibration of cohesive stiffness K_{IP}, cohesive strength σ_c, and fracture energy G_c. The CZM is considered as nonlinear spring foundation. The DCZM for line type crack (DCZM2D) has been established [8-11]. The previous studies have shown that DCZM2D is not sensitive to the FEM mesh size and computational efficient. This paper further extends DCZM into surface type cracks (DCZM3D). It is a promising tool to perform crack growth analysis for none linear material softening.

2. Methodology

2.1 Kinematics Relations

To apply DCZM, nonlinear springs are embedded among the crack interfaces, which are assumed to debond. Figure 3(a) shows one such spring located between two

nodes: node 1 and node 2 on the crack front. Nodes 3 to 6 are introduced to compute effect area and construct local coordinate system. They can surround either node 1 or node 2 (as shown in Figure 3(a)). Obviously, the effect area for DCZM is:

$$\Delta A = \frac{1}{2} A_{3456} \qquad [4]$$

where ΔA and A_{3456} are the DCZM affected area and the area enclosed by nodes 3 to 6, respectively.

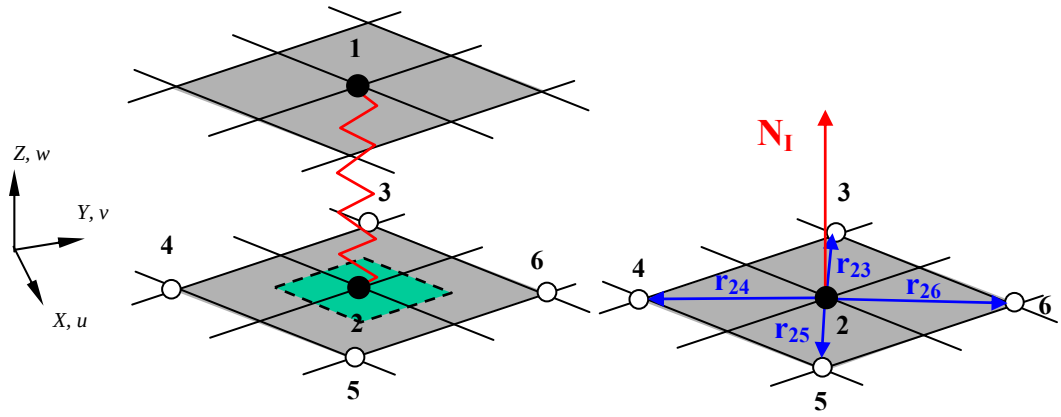

Figure 3. Effective area and local coordinate system

The local coordinate system is constructed as following. First, compute the four vectors that connect the center node 2 to its surrounding nodes (3-6). Refer to Figure 3 (b), we have:

$$\mathbf{r}_{23} = (x_3 - x_2)\mathbf{i} + (y_3 - y_2)\mathbf{j} + (z_3 - z_2)\mathbf{k} \qquad [5]$$

$$\mathbf{r}_{24} = (x_4 - x_2)\mathbf{i} + (y_4 - y_2)\mathbf{j} + (z_4 - z_2)\mathbf{k} \qquad [6]$$

$$\mathbf{r}_{25} = (x_5 - x_2)\mathbf{i} + (y_5 - y_2)\mathbf{j} + (z_5 - z_2)\mathbf{k} \qquad [7]$$

$$\mathbf{r}_{26} = (x_6 - x_2)\mathbf{i} + (y_6 - y_2)\mathbf{j} + (z_6 - z_2)\mathbf{k} \qquad [8]$$

Normalize each vector by

$$\mathbf{r} = \frac{\mathbf{r}}{\|\mathbf{r}\|} \qquad [9]$$

$\|\mathbf{r}\|$ is the norm of vector $\mathbf{r}$.

Next, compute the normal vectors for each section that encloses the surface by nodes 3-6. For section enclosed by nodes 2-3-4, its normal vector is

$$\mathbf{N}_I^{34} = \mathbf{r}_{23} \otimes \mathbf{r}_{24} \quad [10]$$

Same computation applies to other three sections (2-4-5, 2-5-6, 2-6-3)

$$\mathbf{N}_I^{45} = \mathbf{r}_{24} \otimes \mathbf{r}_{25} \quad [11]$$

$$\mathbf{N}_I^{56} = \mathbf{r}_{25} \otimes \mathbf{r}_{26} \quad [12]$$

$$\mathbf{N}_I^{63} = \mathbf{r}_{26} \otimes \mathbf{r}_{23} \quad [13]$$

Finally take average over the normal vectors of four sections, we have

$$N_I = \frac{1}{4}\left(\mathbf{N}_I^{34} + \mathbf{N}_I^{45} + \mathbf{N}_I^{56} + \mathbf{N}_I^{63}\right) \quad [14]$$

Normalize it and we have the unit vector of the surface enclosed by nodes 3-6.

$$\mathbf{n}_I = \frac{\mathbf{n}_I}{\|\mathbf{n}_I\|} \quad [15]$$

2.2 Nonlinear Springs

Three springs between node 1 and node 2 (crack tip) in global coordinate system (*X*, *Y*, *Z*), respectively. K_x, K_y, and K_z are the spring stiffness for each direction. The nodal force ($\mathbf{F}$) and displacement opening ($\boldsymbol{\Delta}$) in the global system (X, Y, Z) between node 1 and node2 can be computed by.

$$\boldsymbol{\delta} = (u_1 - u_2)\mathbf{i} + (v_1 - v_2)\mathbf{j} + (w_1 - w_2)\mathbf{k} \quad [16]$$

$$\mathbf{F} = K_x(u_1 - u_2)\mathbf{i} + K_y(v_1 - v_2)\mathbf{j} + K_z(w_1 - w_2)\mathbf{k} = \mathbf{K}\boldsymbol{\delta}^T \quad [17]$$

where $\mathbf{K} = \begin{bmatrix} K_x & 0 & 0 \\ 0 & K_y & 0 \\ 0 & 0 & K_z \end{bmatrix}$ [18]

Project nodal force ($\mathbf{F}$) and displacement opening ($\boldsymbol{\Delta}$) into the local coordinate system ($\mathbf{n}_I$) for mode I, we have

$$F_I = \mathbf{F} \cdot \mathbf{n}_\mathbf{I} \quad [19]$$

$$\delta_I = \boldsymbol{\delta} \cdot \mathbf{n}_\mathbf{I} \quad [20]$$

2.3 Mode I Cohesive Law

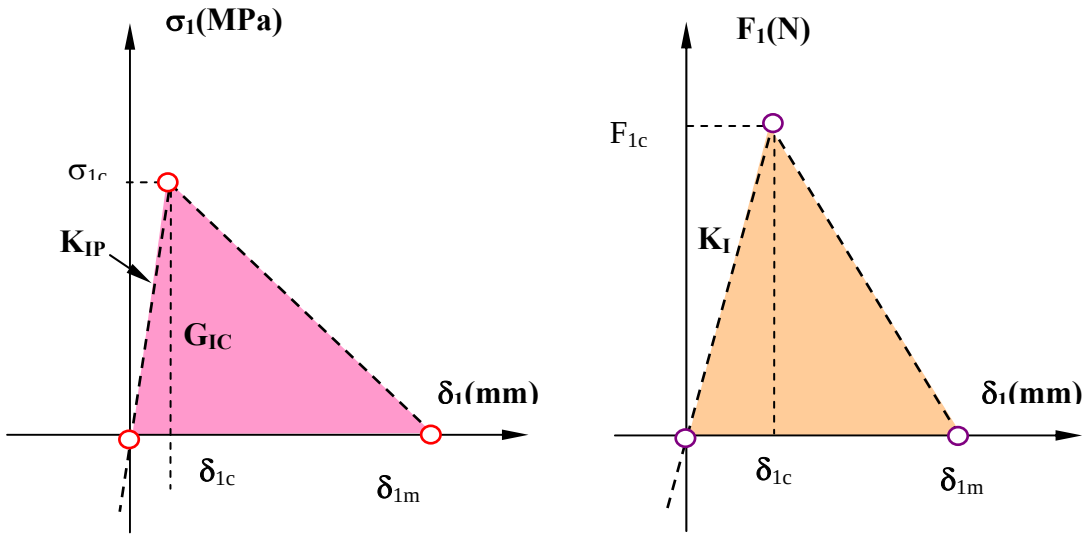

Figure 4. DCZM-fracture element and local coordinate system

In CZM, for pure mode I, the direct inputs are cohesive strength σ_{1C}, fracture energy G_{1C} and cohesive stiffness K_{1P}. They are standard SI units are N/mm^2, N/mm, and N/mm^3. Refer to Figure 4(a), we can compute the critical opening (δ_{1C}) and the maximum opening (δ_{1m}) as:

$$\delta_{1C} = \frac{\sigma_{1C}}{K_{1P}} \qquad [21]$$

$$\delta_{1m} = \frac{2G_{IC}}{\sigma_{1C}} \qquad [22]$$

In the spring, we need the nodal cohesive force (F_{1C}) and the spring stiffness (K_1) and they can be computed by:

$$F_{1C} = \sigma_{1C}\Delta A \qquad [23]$$

$$K_1 = \frac{F_{IC}}{\delta_{1C}} = \frac{\sigma_{IC}\Delta A}{(\sigma_{IC}/K_{IP})} = K_{IP}\Delta A \qquad [24]$$

2.4 Apply the cohesive zone law

For pure mode I, the nonlinear spring will behave as following based on the crack opening, δ_1:

If $\delta_1 < \delta_{1C}$: $K_1 = K_{IP}\Delta A$ [25]

If $\delta_{1C} < \delta_1 < \delta_{1m}$: $K_1 = \left(\frac{\delta_{1m}}{\delta_1} - 1.0\right)\frac{F_{1C}}{\delta_{1m} - \delta_{1C}}$ [26]

If $\delta_1 > \delta_{1m}$: $K_1 = 0.0$ [27]

3. Results

The above DCZM-surface crack (DCZM3D) for pure mode I has been implemented into GENOA-PFA. Several examples have been examined to validate the approach and verify the implementation.

3.1 CCZM and DCZM

Figure 5 shows the mesh preparations from GENOA-DCZM and ABAQUS-CCZM, In the DCZM, respectively. In DCZM, two node sets are collected from top and bottom surfaces. GENOA-DCZM will automatically match the corresponding node pairs and apply DCZM. In CCZM, continuum type elements are inserted between top and bottom surfaces. Therefore, CCZM is not as convenient as DCZM in mesh preparation.

Since DCZM uses springs, it has no restrictions on the gap dimension. Therefore, it is super when applied to analyze crack growth within very thin adhesive layers. For CCZM, very thin elements have bad element aspect ratios, which way lead to convergence troubles.

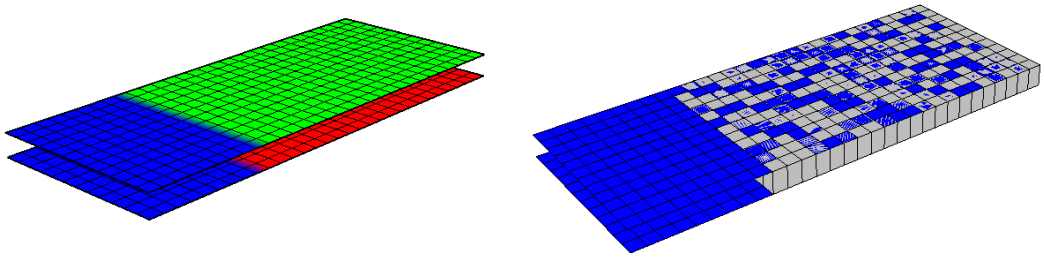

Figure 5. DCZM and CCZM mesh preparation

Figure 6 shows the comparisons between DCZM and CCZM. Figure 6(a) gives the CZM laws with fracture energy $G_{Ic} = 0.2\text{N/mm}$; cohesive strength $\sigma_{Ic} = 1.85\text{MPa}$ and cohesive stiffness $K_{IP} = 50.0\text{NMPa}$. Figure 6(b) shows the ultimate load with respect to the element numbers (convergence study). It can be seen that DCZM is almost a horizontal line, which indicates that DCZM is not sensitive to the FEA mesh size. The DCZM (GENOA) converges to 3.39N while CCZM (ABAQUS) converges to 3.22N. The relative error for this example is about +5%. This comparison indicates DCZM and CCZM can be equivalent to each other. Figure 6(c) and Figure 6(d) show the load vs. deflection curves obtained from DCZM(GNEOA) and CCZM(ABAQUS), respectively.

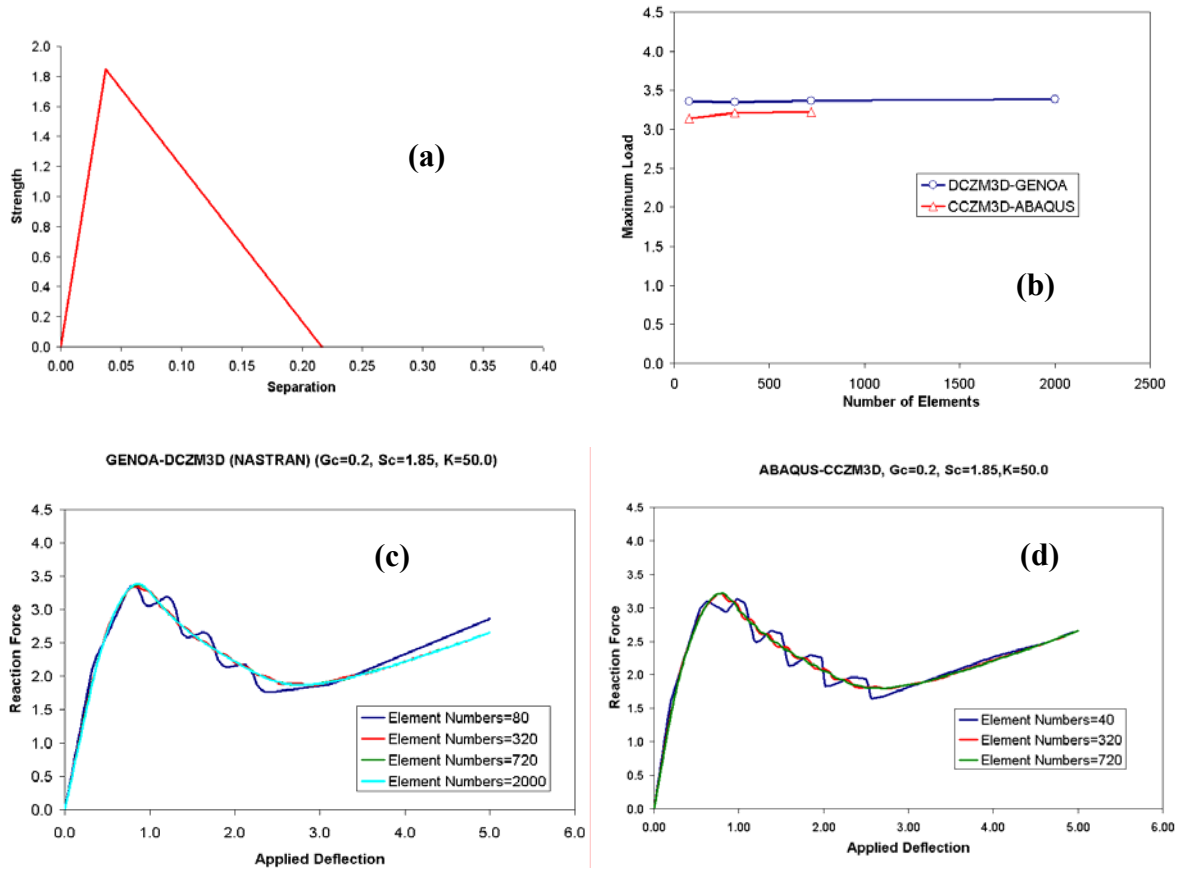

Figure 6. Comparisons between DCZM and CCZM

3.2 VCCT, DCZM2D and DCZM3D

Next, the Crisfield DCB specimen was studied by DCZM3D (surface crack) presented in this paper. It was also studied previously in [11] by using VCCT and DCZM2D (line crack). Figure 7 shows all these results. It can be seen that DCZM3D has a close curve to DCZM2D. This means that, for this particular example, DCB can be modeled by 2D model and the 3D effect is negligible.

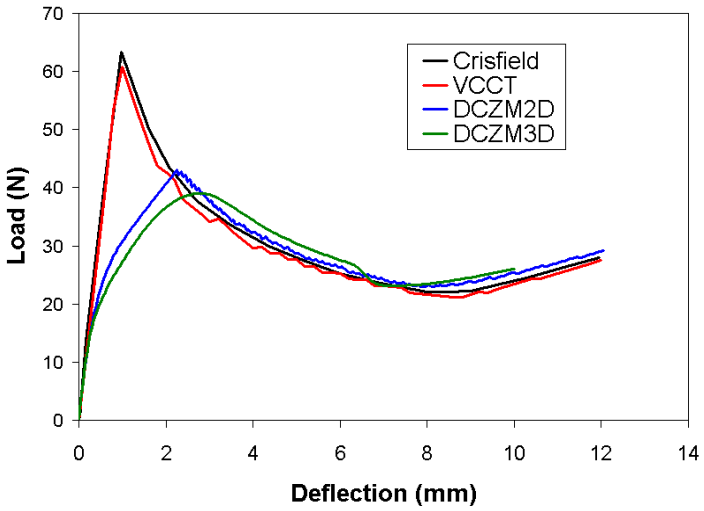

Figure 7. Comparisons among VCCT, DCZM2D and CCZM3D for Crisfield DCB specimen

3.3 Shell Element Model and Solid Element Model

This DCB (Double cantilever beam) example was used to validate the approach by modeling DCB with shell elements and solid elements, respectively. Figure 8 shows the FEM meshes. Figure 9 shows the load vs. deflection curves for both models.

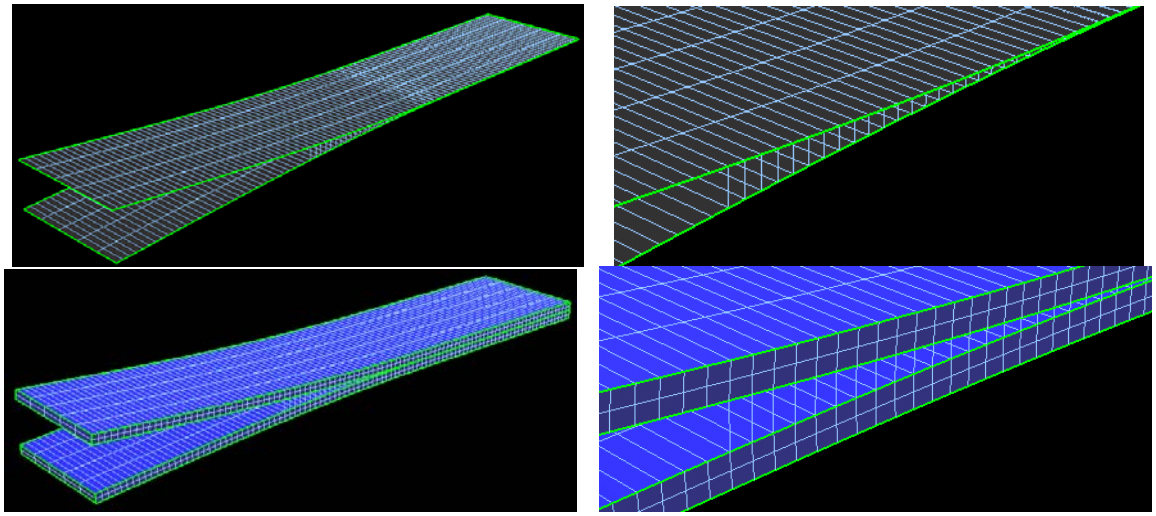

Figure 8. Shell and Solid modeling of DCB with DCZM3D

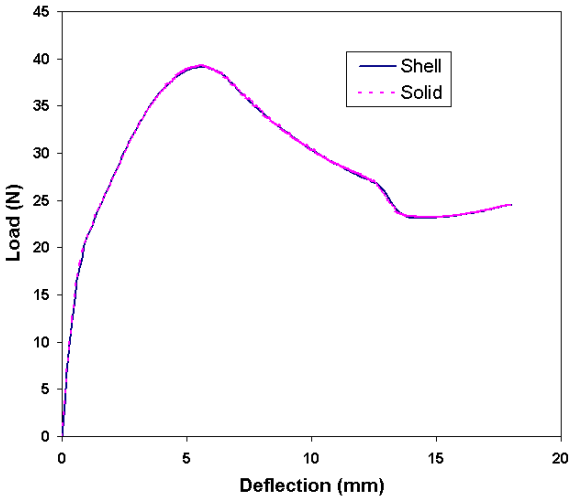

Figure 9. Comparison between shell model and solid model

3.4 Composite Storage Module Joint Analysis and Test Verification

The General Dynamics Composite Storage Module (CSM) joint was a particularly useful example structure as a thorough analysis and testing program accompanied the design and verification of the joint development. A significant portion of this program was developed into a paper [16]. The CSM joint version of interest was composed of a graphite/epoxy quasi-isotropic laminate adhesively bonded to a tapered titanium fitting. The CSM and joint details are shown in Figure 10. Details of the FE model and materials used in the analysis are shown in Figure 11. The test indicated that the primary failure mode of the joint was adhesive failure within the EA9394 [17] layer between the titanium and fiberglass.

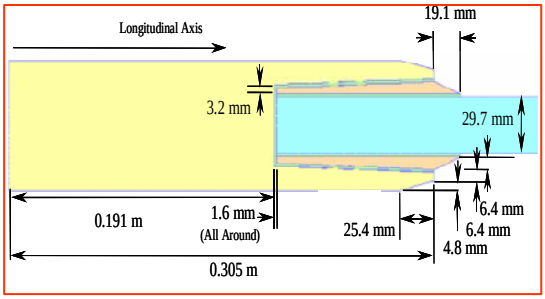

a) CSM Configuration

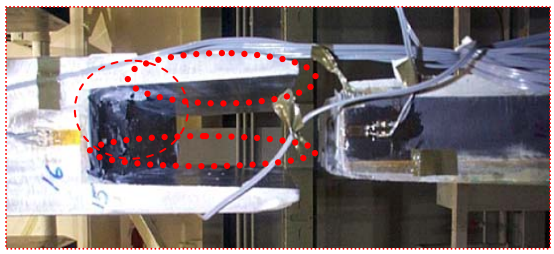

b) Relatively Clean Ti Interface Indicates a Premature Adhesive Failure

Figure 10. Composite Storage Module and joint geometry (CSM)

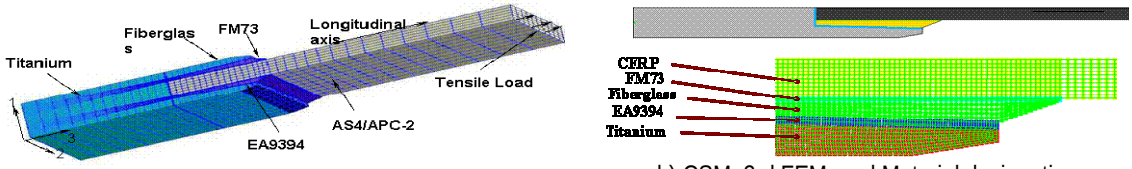

a) CSM 3-d FEM: material, load direction

b) CSM 2-d FEM, and Material designation

Figure 11. FE model details and materials for PFA, and VCCT

Several steps were taken before the final GENOA Progressive Failure Analysis (PFA) was performed in order to develop and demonstrate confidence in the software. As a baseline check, linear analyses were performed using standard FEA software packages ANSYS and ABAQUS along with GENOA. Results along the adhesive centerline of the EA9394 adhesive are shown in Figure 12a. The validation of simulation results to capture the nonlinear material behavior of the adhesive was achieved by duplicating the ABAQUS analysis performed by General Dynamics. The tensile equivalent (Von Mises) stress near the free edge of the EA9394 is plotted versus the total applied load for both analyses in Figure 12b.

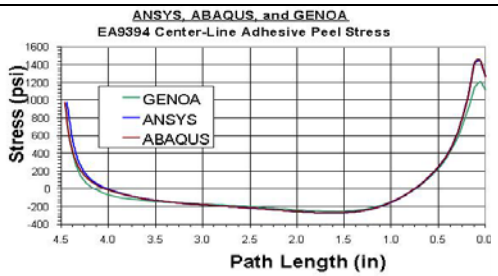

a) Comparison of Centerline Peel Stress Predictions Within the (Linear) EA9394

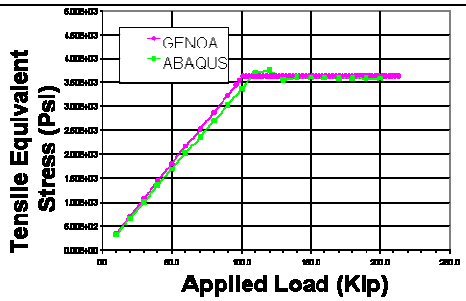

b) Tensile Equivalent Stress History Prediction Comparison Between ABAQUS and GENOA

Figure 12.CSM Model Code Verification

A full PFA was performed and compared to the test data. The predicted load deflection curve and associated damage mechanisms are shown in Figure 13. While the failure mechanisms predicted by the analysis were very similar to those observed during the test (Figure 13b), the analysis predicted a much higher strength for the joint (see Figure 13a). This was attributed to the maximum value of strain the adhesive could withstand and the surface preparation of the titanium. Subsequent review of the failure surfaces revealed a clean titanium surface indicating a premature interfacial failure of the adhesive to titanium bond (Figure 10b). A relatively inexpensive coupon-level test of the titanium prepared as for the CSM joint coupon would yield a more relevant value of adhesive strength/strain limit for use in future analyses.

The analysis was re-run to introduce the Clean surface interfaces on Ti fitting (test suggest adhesive failure as opposed to cohesive failure) using: 1) Virtual Crack Closure Technique (VCCT), and 2) degrading the adhesive properties using 20% void formation, as shown in Figure 14. VCCT required a predetermined crack path, and was modeled in

two ways: a) multiple crack location, and single crack initiation point. For these simulations the crack path was determined from PFA (Figure 13b). The results obtained predicted similar strength value as predicted by PFA strength based analysis. Plain strain fracture toughness (K_{1C} and K_{IIC}) values were required to run analysis using VCCT approach. The K_{1C} and K_{IIC} values were obtained from literature for EA9394 adhesive [17]. PFA predictions are usually close but are not considered precise when pre-cracked conditions exist in a simulation due to infinite stresses near a sharp crack tip.

Thereafter to capture the effect of improper bonding, the VCCT was defined on limited node pairs as shown in Figure 14a. The trend of the results indicated that the defining the partial bonding can simulate the effect of improper bonding, as shown in Figure 14b.
Similarly higher void (~20%) was used to simulate the improper bonding in PFA. Again the results were found to be a close match with that of the test (see Figure 15). In conclusion, if proper contact surface area information is available before the analysis, PFA and VCCT can be used judicially to simulate the effect of improper bonding. Also, that improper bonding can be modeled by varying the voids percentage in the adhesive to simulate the improper bonding scenario if surface area is not available.

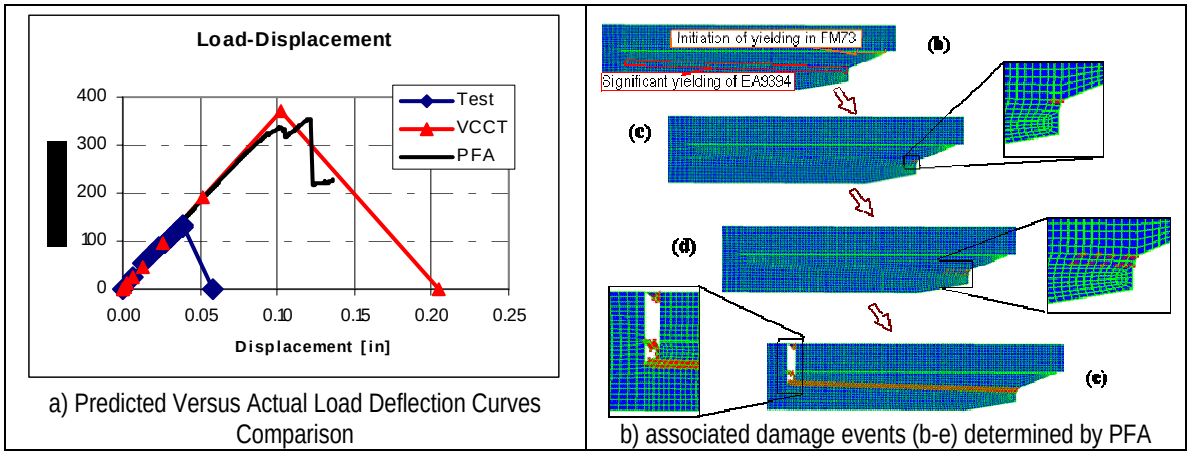

a) Predicted Versus Actual Load Deflection Curves Comparison

b) associated damage events (b-e) determined by PFA

Figure 13. Predicted load-deflection curve and associated damage events

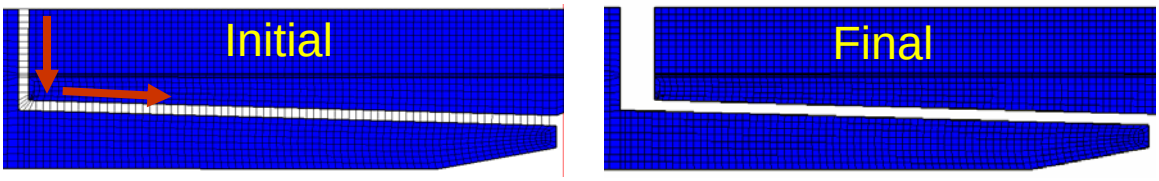

a) VCCT approach to simulate complete bonding. Crack initiates from the left and propagates towards right

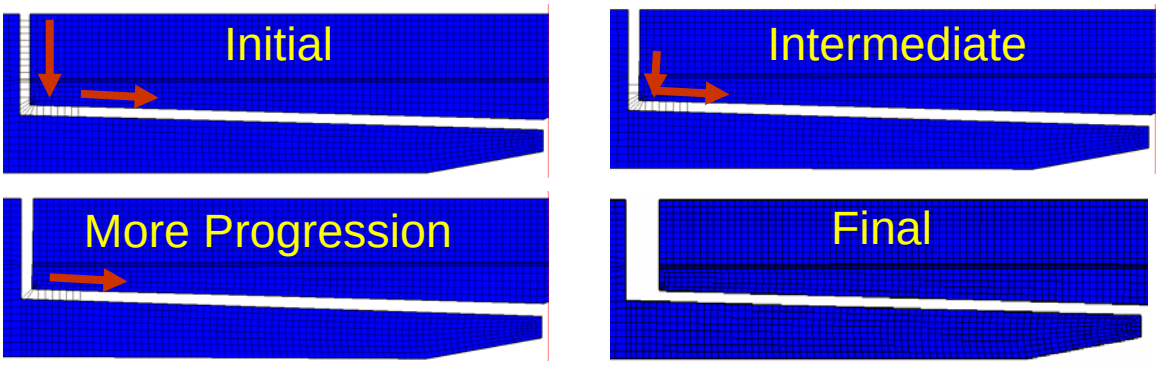

b) Partial VCCT approach to simulate partial (improper) bonding

Figure 14. a) Single VCCT approach, b) Partial Single VCCT approach to simulate partial (improper) bonding.

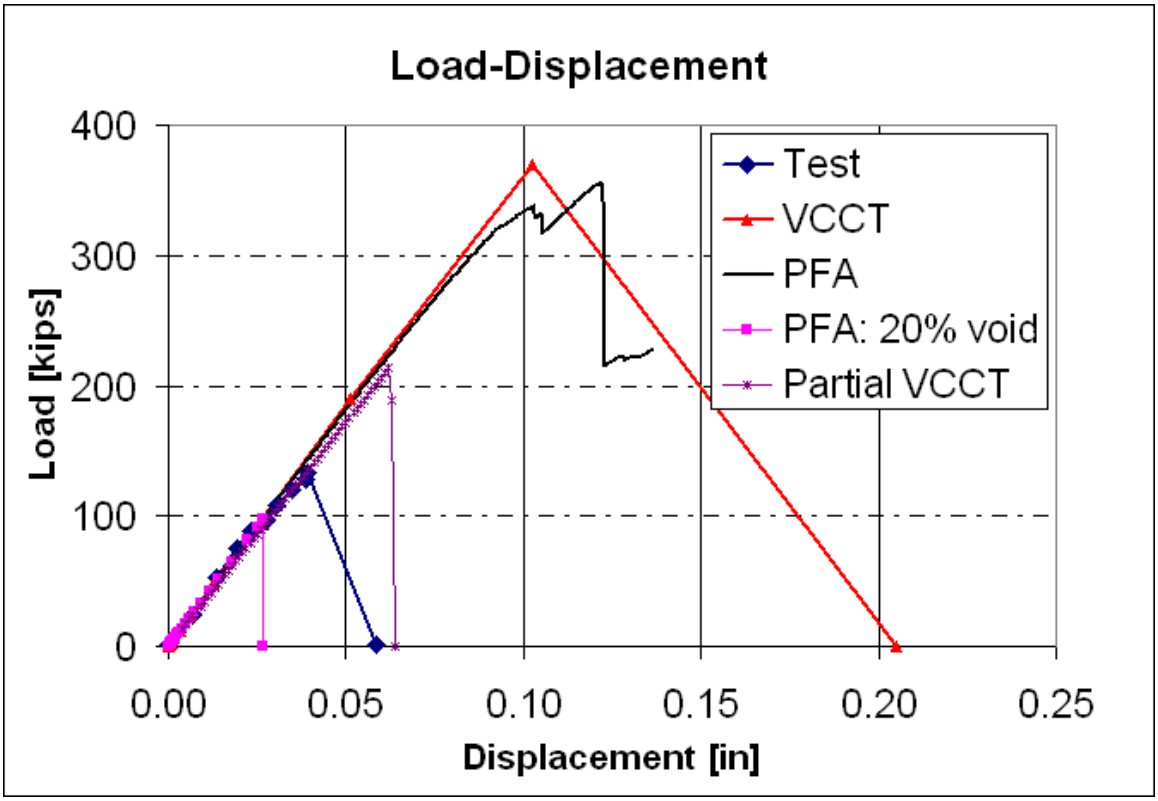

Figure 15: Comparison of the simulated load displacement curve with test data.

4. Conclusion

A combined finite element (FE) based strength/strain based Progressive Failure Analysis, along with non-predetermined interfaces and Continuous/Discrete Cohesive Zone Model (CZM) of fracture interface elements along predetermined interfaces methodology have been developed that enable the practical application of the crack growth. Method development considered both 2D (crack tip) and 3D (crack front) implementations, specifically where non-linear behavior occurs in the model, or if crack propagation predictions are desired.

Several comparative studies of these methodologies against the other FE codes and test data were performed. It was concluded that in a very thin adhesive layer application: a) DCZM software, which uses spring elements and has no restrictions on the gap dimension, will automatically match the corresponding node pairs and apply DCZM; b) in CCZM, continuum type elements are inserted between top and bottom surfaces. Therefore, CCZM is not as convenient as DCZM in mesh preparation. Generation of very thin elements with high aspect ratios may lead to convergence troubles.

In the Composite Storage Module (CSM) adhesively bonded joint tests revealed pre-mature failure of the bonded area that was a possible combination of both adhesive and cohesive failure. Adhesive joint failure was caused by a) non-clean joint surface preparation, b) thick bond lines, and c) existence of void in the adhesive bondline. This problem was analyzed using two approaches: a) Progressive failure analysis with

complete and partial bond void representation and b) Virtual Crack Closure Technique with complete and partial bonding. The analytical results predicted full load carrying capability of the joint using PFA and VCCT complete bondline approach and a significant reduction in the load carrying capability due to improper bonding.

References

1. Xie D and Biggers, Jr. SB, Progressive crack growth analysis using interface element based on the virtual crack closure technique, *Finite Elements in Analysis and Design*, 42(2006): 977-984.
2. Xie D and Biggers, Jr. SB, Strain energy release rate calculation for a moving delamination front of arbitrary shape based on virtual crack closure technique, Part I: Formulation and Validation, *Engineering Fracture Mechanics*, 73(2006): 771-785.
3. Xie D and Biggers, Jr. SB, Strain energy release rate calculation for a moving delamination front of arbitrary shape based on virtual crack closure technique, Part II: Sensitivity Study on Modeling Details, *Engineering Fracture Mechanics*, 73(2006): 786-801.
4. Xie D and Biggers, Jr. SB, Delamination growth and residual strength of compressively loaded sandwich panels with stiffness tailored face sheets, *Journal of Sandwich Structures and Materials*, in press.
5. Mabson, G.E., Deobald, L.R. and Dopker B., Fracture interface elements for the implementation of the virtual crack closure technique, In: *48th AIAA/ASME/ASCE/AHS/ASC structures, structural dynamics & materials conference*, AIAA-2007-2376, Honolulu, HI, April 23–26, 2007.
6. Farahmand B, Saff C, Xie De, and Abdi F, Estimation of fatigue and fracture allowables for metallic materials under cyclic loading, *48h AIAA/ASME/ASCE/AHS/ASC Structures, Structural Dynamics & Materials Conference*, AIAA-2007-2381. Honolulu, Hawaii. April 23-26, 2007.
7. Deobald, L.R., Mabson, G.E., Dopker B., Hoyt D.M., Baylor, J. and Graesser D. Interlaminar fatigue elements for crack growth based on virtual crack closure technique, In: *48th AIAA/ASME/ASCE/AHS/ASC structures, structural dynamics & materials conference*, AIAA-2007-2091, Honolulu, HI, April 23–26, 2007.
8. Xie D and Waas AM, Discrete cohesive zone model for mixed-mode fracture using finite element analysis, *Engineering Fracture Mechanics*, 73(2006): 1783-1796.
9. Xie D, Salvi AG, Waas AM, Caliskan A, Discrete cohesive zone model to study static fracture of fiber composites, *46th AIAA/ASME/ASCE/AHS/ASC Structures, Structural Dynamics & Materials Conference*, AIAA-2005-2320. Austin, Texas. April 18-21, 2005.
10. Xie D, Salvi AG, Sun C, Waas AM, Caliskan A, Discrete cohesive zone model to study static fracture in a plate of textile braided carbon fiber composites, *Journal of Composite Materials*, 40(2006): 2025-2046.
11. Xie D, Qian J, Huang D, Abdi F, Crack growth strategy in composites under static loading, *47th AIAA/ASME/ASCE/AHS/ASC Structures, Structural Dynamics & Materials Conference*, AIAA-2006-1842. Newport, Rhode Island. May 1-4, 2006.

12. Needleman, A., A continuum model for void nucleation by inclusion debonding. *Journal of Applied Mechanics*, 54 (1987), 525-531.
13. Needleman, A., An analysis of deconhesion along an imperfect interface. *International Journal of Fracture*, 42(1990), 21-20.
14. Chandra, N., Li, H., Shet, C. and Ghonem, H., Some issues in the application of cohesive zone models for metal-ceramic interfaces. *International Journal of Solids and Structures*, 39(2002), 2827-2855.
15. Gao, Y.F., and Bower, A.F., A simple technique for avoiding convergence problems in finite element simulations of crack nucleation and growth on cohesive interfaces. *Modelling and Simulation in Materials Science and Engineering*, 12(2004), 453-463.
16. George F. Leon, Michael F. Trezza, Jeffrey C. Hall,1 and Kelli Bittick, "Evaluation of a Carbon Thermoplastic to Titanium Bonded Joint", ASTM-STP1455-11707.081503.
17. T. R. Guess, E. D. Reedy, M. E. Stavig, 1995. "Mechanical Properties of Hysol EA-9394 Structural Adhesive," *SANDIA REPORT, SAND95-0229 . UC-704.*